

Generation of Quantized Polaritons below the Condensation Threshold

Peter Cristofolini,¹ Z. Hatzopoulos,² Pavlos G. Savvidis,^{2,3,4} and Jeremy J. Baumberg^{1,*}

¹*Nanophotonics Centre, Cavendish Laboratory, University of Cambridge, Cambridge CB3 0HE, UK*

²*FORTH, IESL, 71110 Heraklion, Crete, Greece*

³*Department of Materials Science and Technology, University of Crete, 71003 Heraklion, Crete, Greece*

⁴*Spin Optics Laboratory, Saint-Petersburg State University, 198504, St-Petersburg, Russia*



(Received 6 February 2018; revised manuscript received 27 April 2018; published 7 August 2018)

Exciton polaritons in high quality semiconductor microcavities can travel long macroscopic distances ($>100\ \mu\text{m}$) due to their ultralight effective mass. The polaritons are repelled from optically pumped exciton reservoirs where they are formed; however, their spatial dynamics is not as expected for pointlike particles. Instead we show polaritons emitted into waveguides travel orthogonally to the repulsive potential gradient and can only be explained if they are emitted as macroscopic delocalized quantum particles, even before they form Bose condensates.

DOI: [10.1103/PhysRevLett.121.067401](https://doi.org/10.1103/PhysRevLett.121.067401)

Exciton polaritons are quasiparticles composed of a strongly coupled mixture of excitons and cavity photons confined within a semiconductor microcavity. As long as the carrier densities are well below the Mott transition which ionizes excitons, they behave as composite bosons. The typical de Broglie wavelength of these polaritons is $\lambda_{dB} = \sqrt{2\pi\hbar^2/mk_B T}$ and since the polariton effective mass m is 4 orders of magnitude smaller than that of the exciton due to the distortion of the dispersion by the light-matter coupling, the polariton de Broglie wavelength is more than 100 times larger at the same temperature [1]. In experiments at $T = 5\ \text{K}$, with $5\lambda/2$ -long GaAs microcavities providing a 2D in-plane polariton dispersion $E = ak^2$ [2], where $a = \hbar^2/2m = 0.9\ \text{meV}\mu\text{m}^2$, the polariton $\lambda_{dB} = \sqrt{4\pi a/k_B T} = 5.2\ \mu\text{m}$, while for excitons the corresponding length is a few nm and can be neglected [1]. In this regime polaritons cannot be considered as pointlike particles, and their spatiotemporal dynamics will become dominated by this de Broglie delocalization.

Following the successful demonstration of polariton condensation [3–5], spatially localized reservoirs of excitons can now be created by tightly focused nonresonant optical pumping at high energy [6–14]. This allows a large number of nonlinear phenomena to be accessed including trapped condensates [2,15], phase-locked condensates [16], ring condensates [17], Josephson-coupling [18], superfluidity [19], and more [20,21]. High- k exciton polaritons (“excitons”) can be considered separately from the low- k polaritons which couple to light (see reviews in Ref. [22]). Spatial instabilities can result when polaritons interact with such exciton reservoirs [23,24]. In these systems, however, it remains unclear how the polaritons are emitted by the pumped exciton reservoirs, and exactly how the resulting stable polariton states are chosen.

Here we question how tightly spatially localized excitons can spontaneously emit large wavelike delocalized polaritons. Experiments in a simple geometry clearly show the nonlocal quantum-mechanical size of the polaritons at powers well below the condensation threshold. Excitons are found to emit into polaritons of specific k and direction, set by the quantum confinement. This suggests estimates of polariton interactions based on local polariton density [25] are problematic.

Narrow $50\ \mu\text{m}$ -long lines of excitons are created using a spatial-light-modulator setup [18,26], as either a single line [Fig. 1(a)] or two parallel lines separated by $10\ \mu\text{m}$ [Fig. 1(b)]. Even at the lowest powers, despite uniform exciton populations along the lines created by the 755 nm single-mode cw pump excitation, the emission from the polaritons is found to be localized near the central region of the wires [Fig. 1(b)]. This is completely different from the emission of point particles, which would be dependent only on the local pump power and thus uniform all along the wires.

At around half the condensation threshold [Figs. 1(a), 1(b)], the blueshifts from the lines of excitons already create local potentials U due to the dipole-dipole repulsion of polaritons from excitons. In the case of a single line, this accelerates the polaritons away in both $\pm x$ directions [seen clearly in k -space imaging taken in the Fourier plane [17], Fig. 1(e)], with $\bar{k}_x \sim 1\ \mu\text{m}^{-1}$ corresponding to the $U = a\bar{k}_x^2 = 1\ \text{meV}$ blueshift, and with a wide range of k_y . Comparable polariton velocities are seen when using two pump lines, except that we also now see a distinct population in between the lines which travel only vertically, in the $\pm y$ directions [Fig. 1(f), inside black dashed circles]. Above the global polariton condensation threshold, these behaviors are accentuated, with $\pm x$ outflow for a single line [Figs. 1(c), 1(g), 1(k)], but instead with orthogonal $\pm y$ outflow for two

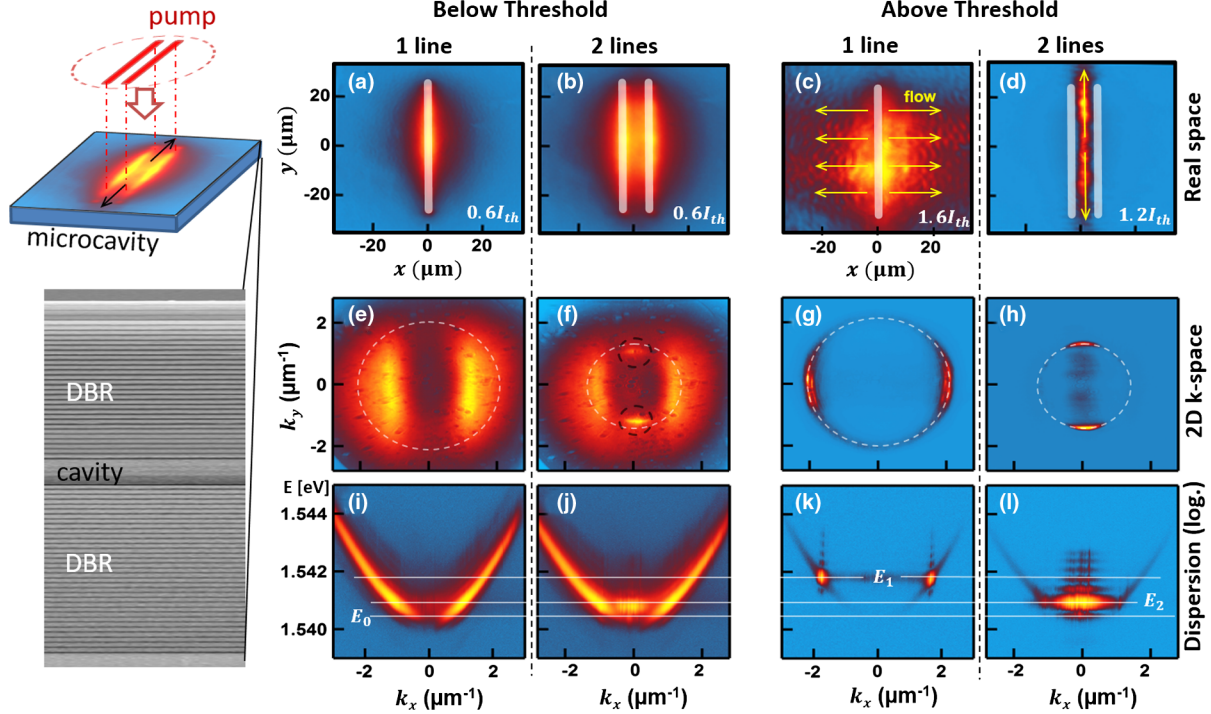


FIG. 1. (a)–(d) Real-space images of polariton emission when pumped with single or pairs of lines (as indicated in left schematic), both below and above the condensation threshold. (e)–(h) Corresponding momentum-space images of the entire polariton emission, white circles mark eventual condensation wave vector. (i)–(l) Cuts of the $E(k)$ dispersion across the center of the dashed circles marked in (e)–(h).

lines [Figs. 1(d), 1(h), 1(l)]. For two pump lines, *all* polaritons are now created inside this “waveguide” traveling as jets in $\pm y$ with no emission outside the lines. As we will show below, these different behaviors arise from the different polariton spatial wave functions in the two cases, and how pointlike excitons emit into them. We note also the condensate blueshift is much smaller for two lines (E_2) compared to a single line (E_1) above threshold [Figs. 1(k), 1(l)].

These properties are clarified in the cross sections of Fig. 2. At the lowest powers (blue), polaritons traveling sideways from a single line (to $\pm x$) exponentially decay as they leak through the cavity mirrors at a constant rate given by $\tau_c = 12$ ps, thus ballistically propagating a distance $l_c = \tau_c v = \tau_c \sqrt{2U/m} = 2ak\tau_c/\hbar \sim 5 \mu\text{m}$. Measuring the distribution along the pump line, however, instead of a nearly flat density matching the exciton reservoir (seen via low power exciton luminescence [2,26]), the polariton profile is almost Gaussian [Figs. 2(b), 2(d)] and the density at each end (vertical lines) is 10 times lower than expected from a local emission picture. Artifacts from optics cannot explain these results since they do not depend on the orientation of the lines on the sample (which can be arbitrarily changed without effect), while blurring from defocus could not simultaneously account for the $5 \mu\text{m}$ FWHM in the x direction with the $42 \mu\text{m}$ FWHM in the y direction. Exciton diffusion (which is only a few microns in

any case [27]) would also blur the polariton distributions similarly in x and y , completely different from what is seen. Equivalent results are seen at low power with two pump lines, although now large polariton populations start to collect in the trap between the lines, accelerating along $\pm y$. These effects occur in the linear regime with no power dependent changes in the real-space distribution along the line being observed until reaching threshold [Figs. 2(b), 2(d)]. At higher powers above threshold, the second order transverse mode of this polariton waveguide is observed [Fig. 2(c), top curve]. Since higher order transverse modes are also seen for larger separations between the pump lines, we keep the pump spacing fixed. A first question is thus to understand what controls the shape of the polariton emission along the pump-induced wires.

The second observation to explain is what is seen in k space for polaritons in between the two lines [Figs. 2(f), 1(f), 1(h)]. For a single pump line [Fig. 2(e)] the k space shows the polaritons accelerated either way in $\pm x$. As the exciton reservoir population rises the exciton blueshifts increase, thus increasing the kinetic energy of the polaritons emitted. However, for two pump lines we now find polaritons increasingly accelerated along the waveguide in between the pump lines in the $\pm y$ directions. In a simple classical point-particle emission picture, polaritons created at the top of the potential hill where the excitons are located would roll down along $\pm x$ into the intervening valley and

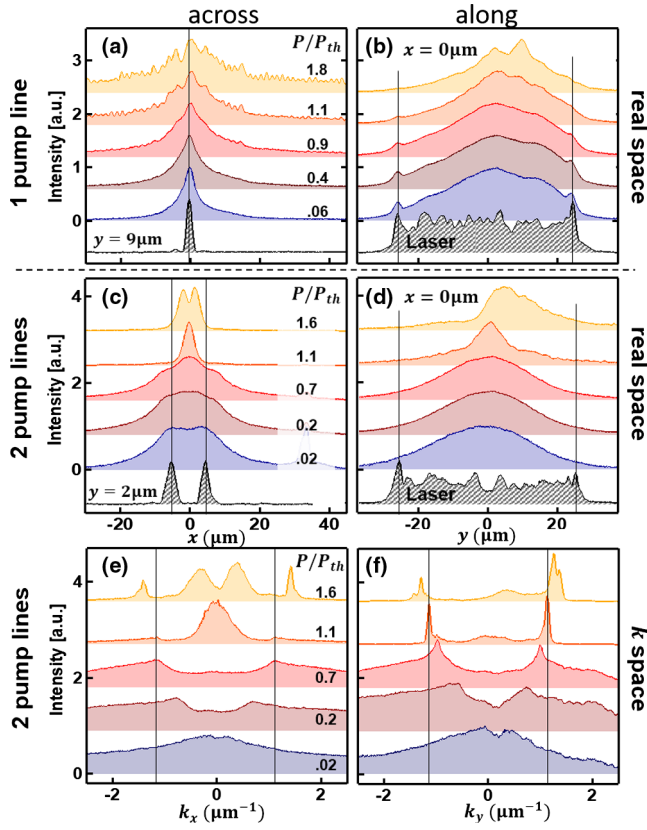


FIG. 2. (a)–(d) Real-space cuts of the polariton distributions (a) across and (b) along a single pump line, (c) across and (d) along two pump lines, for increasing pump powers. Gray lines show measured excitation profiles (speckle contributes noise). (e), (f) Corresponding cuts along k_x and k_y for two pump lines.

up the other side before reversing their trajectory. Nor would including classical polariton collisions give the $\pm k_y$ directed distributions. In the quantum delocalized situation, instead polaritons are directly created traveling in the orthogonal directions along $\pm y$.

This acceleration in y along the polariton waveguide can be directly seen, by focusing the emitted light at an intermediate image plane and selecting emission from only a specific spatial region using a pinhole (Fig. 3, yellow circles). Along the waveguide [Figs. 3(a), 3(b)] the polariton velocity increases from zero in the center, caused by the increasing blueshift U_0 of these polaritons as the pump power is increased [Fig. 3(c)], with $k_y^{\max} = \sqrt{U_0/a}$. As polaritons move vertically, their potential energy is converted into kinetic energy, keeping their total energy constant [Fig. 3(d)]. Clear evidence of separation between polaritons inside and outside the waveguide is seen in Fig. 3(h), where the energy of the trapped polaritons is up to 400 μeV below the energy at the reservoir walls. Although the exciton reservoir is well separated from the center of this waveguide, the delocalized shape in Fig. 2(c) of the lowest order polariton mode $\psi_1(x)$ overlaps with the exciton reservoir, resulting in a

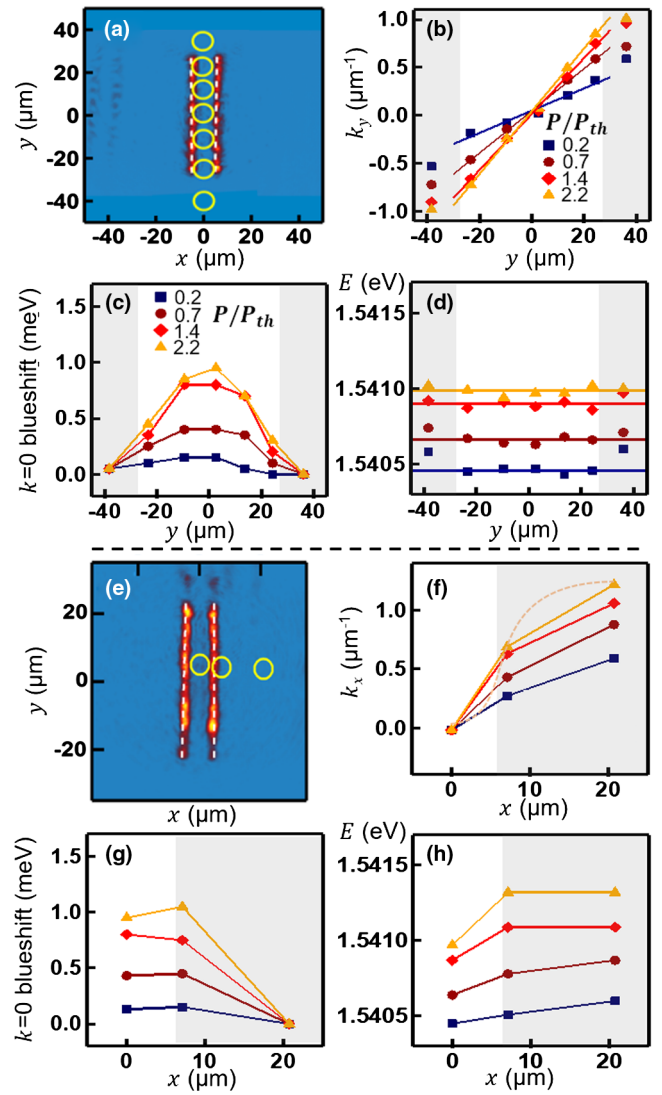


FIG. 3. Spatially resolved and energy-resolved polariton emission using two pump lines, scanned along (a)–(d) the y and (e)–(h) x directions. (a,e) Images of pump laser, yellow circles mark pinhole positions. (b)–(d) Polariton momentum, local blueshift energy, and absolute energy for positions in (a) along y , (f)–(h) equivalent along x . Regions outside the polariton waveguide are shaded gray.

net blueshift. Surprisingly, however, this blueshift decreases as the polaritons travel vertically along y [Fig. 3(c)] and seems to match the observed distribution of polaritons along the lines [Figs. 1(a), 1(b), 2(b), 2(d)], despite the uniform density of excitons along the lines. This evidences the large spatial size of emitted polaritons, which corresponds to the length of the wires. Such observations can potentially account for recent suggestions that blueshifts from polariton populations are anomalously large [25].

We explore an explanation that accounts for these observations. If polaritons accelerated by the 1 meV blueshifts only travel for 5 μm before radiating, the 25 μm polariton path observed along the waveguide cannot be

purely ballistic. This drift length is comparable with the de Broglie wavelength of the polaritons. An alternative picture is that there are a range of quantized polariton states that exist in the waveguide, and excitons emit preferentially into the lowest $n = 1$ state. In this picture confinement is provided by localized gain $G(y)$ from the exciton line reservoirs as well as their blueshifts $V(y)$. Solving the time-independent Schrodinger equation in one dimension but now for complex potentials so that $\tilde{V} = V(y) + iG(y)$, we find that bound states exist (with the energy poles in the upper half of the complex plane) if there is net gain $G_{\text{eff}} > 0$ (accounting for gain and loss) in some region, independent of the values of V (which can be repulsive too). Taking this simple 1D system with $\tilde{V}(|y| < 15 \mu\text{m}) = 1 \text{ meV} + i0.5 \text{ meV}$ and with additional uniform (radiative) loss everywhere of $-i0.25 \text{ meV}$ [Fig. 4(a)], we solve using a transfer matrix formalism to locate the bound states in the complex frequency plane [Fig. 4(b)] [1,28]. Despite the strong repulsive potential (given by the blueshift potential), bound states are supported in this system (gray curves, plotted at their respective eigenenergies), with the lowest state looking remarkably similar to the low-pump-power PL profile in Figs. 1, 2. The polaritons are also fully confined in the lateral direction (x) in the lowest mode.

The large size of the quantized polariton states observed is directly related to the extremely small effective mass of polaritons. The highly localized excitons are confined to the pump lines but emit polaritons into these nonequilibrium extended quantized states. This shows that a system with effective gain can express stationary states localized to the gain area, analogous to those found in a finite potential well. We note that numerical simulations have shown that the Schrödinger equation in the presence of gain (i.e., a positive imaginary potential) indeed behaves similarly to the nonlinear electromagnetic wave equation, and a system with sufficient gain becomes insensitive to time-dependent perturbations [29]. This is also analogous to descriptions of spatial solitons in a driven-dissipative system [30].

An intriguing aspect to these observations is that the quantized polariton states have a (real) energy spacing from the confinement along the waveguide (y), which is of order

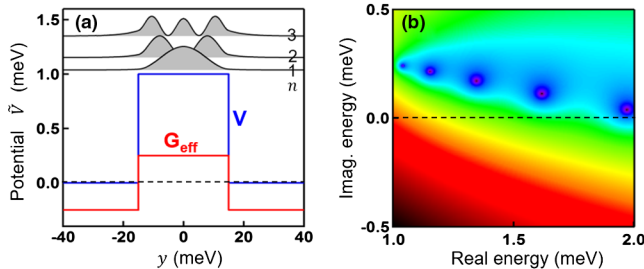


FIG. 4. (a) Bound states in a repulsive potential (blue) with effective gain (red). Gray shaded curves show the first three quantum states plotted at the respective eigenenergies. (b) Corresponding poles in the complex energy plane.

0.1 meV. Since typical thermal energies at 10 K are 0.8 meV, in thermal equilibrium we would expect at least the five lowest states to fill with polaritons. This would mean that their spatial distribution would no longer follow the Gaussian-like distribution of the lowest $n = 1$ state, which is, however, clearly seen. At the same time, $\Im m(E) \approx G_{\text{eff}}(0)$ is of the same order, giving relaxation rates of these states $\hbar/\tau_c = 0.1 \text{ meV}$ on the order of the energy spacing. Our data thus suggest that polaritons are already preferentially injected into the lowest coherent state, even below threshold. It thus appears that nonlinear polariton interactions select the lowest state, even though enough thermal energy is available for excitation into the higher states (i.e., this is a nonequilibrium not a thermal effect).

To check the coherence directly we examine the polaritons inside the waveguide which are linearly accelerating out from the center towards both ends [Figs. 3(b), 1(b), 1(d)]. Since there is no abrupt change of dynamics at the condensation threshold, this poses the question whether coherence is established already below condensation. We experimentally address this by performing Young's slit interferometry on the light emitted from between the two pumped lines [Fig. 5(a)]. We use two pinholes with variable separation δ placed in an intermediate real space plane to collect light from two distant regions (diameter $3.8 \mu\text{m}$) and interfere them in the far field [31]. Spatial coherence between the two selected regions shows up in k space as

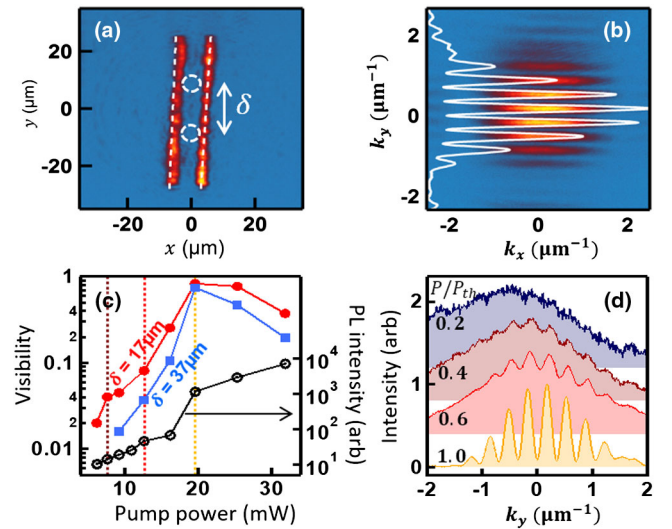


FIG. 5. Coherence of the waveguided polaritons as a function of pump power. (a) Image of pump laser lines with location of pinholes (as positioned in intermediate real space plane). (b) Double pinhole interference pattern formed in the far field for a condensate. (c) Pump power dependence of the fringe visibility for two pinhole separations δ , with integrated emission (black curve). (d) Fringe cross section for $\delta = 17 \mu\text{m}$ at increasing pump powers, highlighted by dashed lines in (c).

interference fringes [Fig. 5(b)]. The fringe contrast measures the degree of coherence as a function of pump power [Figs. 5(c), 5(d)] for different pinhole separations as indicated. We note that $\delta = 17$ and $37 \mu\text{m}$ are ~ 4 and 8 times the de Broglie wavelength $\lambda_{\text{dB}} \simeq 5 \mu\text{m}$. The decrease in visibility above the condensation is due to formation of multiple condensates at higher energies. In all cases the rise of coherence with pump power is exponential, appearing even below $0.3P_{\text{th}}$. The $n = 1$ state into which polaritons are emitted supports their coherent propagation in both $\pm y$ directions and appears to be a linear (i.e., one-polariton) rather than a nonlinear (two-polariton) effect. Our data thus show that individual polaritons have to be considered as delocalized coherent quantum objects, even before they collectively condense. Their properties thus do not arise from their local density, local emission, or local interactions.

In summary, we have shown that well below threshold, gain guided polaritons occupy discrete quantized states and exhibit coherence, even where their level spacings are much less than thermal energies. Localized excitons which weakly overlap with the $n = 1$ polariton state can emit into polariton superpositions that travel coherently in $\pm y$ directions. Spatial correlations are visible already at a fraction of the condensation threshold power, suggesting that coherence is intrinsic to the population of waveguided polaritons. These results also suggest great care must be taken in considering the blueshifts of polaritons, given how polariton wave functions are gain guided by the surrounding exciton populations.

This work is supported by UK EPSRC Grants No. EP/G060649/1, No. EP/L027151/1 and ERC Grant No. LINASS 320503. P.G.S. acknowledges Saint-Petersburg State University research grant 11.34.2.2012 and AENAO project co-financed by EU ERDF and Greek NSRF 2014–2020 funds.

*jjb12@cam.ac.uk

- [1] A. V. Kavokin, J. Baumberg, G. Malpuech, and F. P. Laussy, *Microcavities* (Oxford Univ. Press, Oxford, 2007).
- [2] G. Tosi, G. Christmann, N. G. Berloff, P. Tsotsis, T. Gao, Z. Hatzopoulos, P. G. Savvidis, and J. J. Baumberg, *Nat. Phys.* **8**, 190 (2012).
- [3] H. Deng, G. Weihs, C. Santori, J. Bloch, and Y. Yamamoto, *Science* **298**, 199 (2002).
- [4] J. Kasprzak, M. Richard, S. Kundermann, A. Baas, P. Jeambrun, J. M. J. Keeling, F. M. Marchetti, M. H. Szymańska, R. André, J. L. Staehli *et al.*, *Nature (London)* **443**, 409 (2006).
- [5] G. Christmann, R. Butté, E. Feltn, J.-F. Carlin, and N. Grandjean, *Appl. Phys. Lett.* **93**, 051102 (2008).
- [6] C. Schneider, K. Winkler, M. D. Fraser, M. Kamp, Y. Yamamoto, E. A. Ostrovskaya, and S. Höfling, *Rep. Prog. Phys.* **80**, 016503 (2017).
- [7] E. Wertz, L. Ferrier, D. D. Solnyshkov, R. Johné, D. Sanvitto, A. Lemaître, I. Sagnes, R. Grousson, A. V. Kavokin, P. Senellart, G. Malpuech, and J. Bloch, *Nat. Phys.* **6**, 860 (2010).
- [8] G. Christmann, G. Tosi, N. G. Berloff, P. Tsotsis, P. S. Eldridge, Z. Hatzopoulos, P. G. Savvidis, and J. J. Baumberg, *Phys. Rev. B* **85**, 235303 (2012).
- [9] J. Fischer, I. G. Savenko, M. D. Fraser, S. Holzinger, S. Brodbeck, M. Kamp, I. A. Shelykh, C. Schneider, and S. Höfling, *Phys. Rev. Lett.* **113**, 203902 (2014).
- [10] J. Schmutzler, T. Kazimierczuk, Ö. Bayraktar, M. Aßmann, M. Bayer, S. Brodbeck, M. Kamp, C. Schneider, and S. Höfling, *Phys. Rev. B* **89**, 115119 (2014).
- [11] M. Pieczarka, M. Syperek, Ł. Dusanowski, A. Opala, F. Langer, C. Schneider, S. Höfling, and G. Sęk, *Sci. Rep.* **7**, 7094 (2017).
- [12] J. Schmutzler, P. Lewandowski, M. Aßmann, D. Niemietz, S. Schumacher, M. Kamp, C. Schneider, S. Höfling, and M. Bayer, *Phys. Rev. B* **91**, 195308 (2015).
- [13] L. Dominici, M. Petrov, M. Matuszewski, D. Ballarini, M. De Giorgi, D. Colas, E. Cancellieri, B. Silva Fernández, A. Bramati, G. Gigli, A. Kavokin, F. Laussy, and D. Sanvitto, *Nat. Commun.* **6**, 8993 (2015).
- [14] D. Ballarini, D. Caputo, C. S. Muñoz, M. De Giorgi, L. Dominici, M. H. Szymańska, K. West, L. N. Pfeiffer, G. Gigli, F. P. Laussy, and D. Sanvitto, *Phys. Rev. Lett.* **118**, 215301 (2017).
- [15] P. Cristofolini, A. Dreismann, G. Christmann, G. Franchetti, N. G. Berloff, P. Tsotsis, Z. Hatzopoulos, P. G. Savvidis, and J. J. Baumberg, *Phys. Rev. Lett.* **110**, 186403 (2013).
- [16] G. Tosi, G. Christmann, N. G. Berloff, P. Tsotsis, T. Gao, Z. Hatzopoulos, P. G. Savvidis, and J. J. Baumberg, *Nat. Commun.* **3**, 1243 (2012).
- [17] A. Dreismann, P. Cristofolini, R. Balili, G. Christmann, F. Pinsker, N. G. Berloff, Z. Hatzopoulos, P. G. Savvidis, and J. J. Baumberg, *Proc. Natl. Acad. Sci. U.S.A.* **111**, 8770 (2014).
- [18] H. Ohadi, Y. del Valle-Inclan Redondo, A. Dreismann, Y. G. Rubo, F. Pinsker, S. I. Tsintzos, Z. Hatzopoulos, P. G. Savvidis, and J. J. Baumberg, *Phys. Rev. Lett.* **116**, 106403 (2016).
- [19] G. Lerario, A. Fieramosca, F. Barachati, D. Ballarini, K. S. Daskalakis, L. Dominici, M. De Giorgi, S. A. Maier, G. Gigli, S. Kéna-Cohen, and D. Sanvitto, *Nat. Phys.* **13**, 837 (2017).
- [20] I. Carusotto and C. Ciuti, *Rev. Mod. Phys.* **85**, 299 (2013).
- [21] D. Sanvitto and S. Kéna-Cohen, *Nat. Mater.* **15**, 1061 (2016).
- [22] I. Carusotto and C. Ciuti, *Rev. Mod. Phys.* **85**, 299 (2013).
- [23] T. C. H. Liew, O. A. Egorov, M. Matuszewski, O. Kyriienko, X. Ma, and E. A. Ostrovskaya, *Phys. Rev. B* **91**, 085413 (2015).
- [24] N. Bobrovskaya, E. A. Ostrovskaya, and M. Matuszewski, *Phys. Rev. B* **90**, 205304 (2014).
- [25] Y. Sun, Y. Yoon, M. Steger, G. Liu, L. N. Pfeiffer, K. West, D. W. Snoke, and K. A. Nelson, *Nat. Phys.* **13**, 870 (2017).
- [26] H. Ohadi, A. Dreismann, Y. G. Rubo, F. Pinsker, Y. del Valle-Inclan Redondo, S. I. Tsintzos, Z. Hatzopoulos, P. G.

- Savvidis, and J. J. Baumberg, *Phys. Rev. X* **5**, 031002 (2015).
- [27] W. Heller, A. Filoramo, P. Roussignol, and U. Bockelmann, *Solid State Electron.* **40**, 725 (1996).
- [28] P. Cristofolini, G. Christmann, S. I. Tsintzos, G. Deligeorgis, G. Konstantinidis, Z. Hatzopoulos, P. G. Savvidis, and J. J. Baumberg, *Science* **336**, 704 (2012).
- [29] H. Bahlouli, A. D. Alhaidari, A. Al Zahrani, and E. N. Economou, *Phys. Rev. B* **72**, 094304 (2005).
- [30] H. Sigurdsson, T. C. H. Liew, and I. A. Shelykh, *Phys. Rev. B* **96**, 115453 (2017).
- [31] F. Dubin, R. Melet, T. Barisien, R. Grousseau, L. Legrand, M. Schott, and V. Voliotis, *Nat. Phys.* **2**, 32 (2006).